Chapter 9

Micro- and Nano-Structuring of Materials via Ultrashort Pulsed Laser Ablation

Chung-Wei Cheng and Jinn-Kuen Chen

Additional information is available at the end of the chapter

http://dx.doi.org/10.5772/intechopen.70454

Abstract

Laser material processing has been demonstrated as an effective means for machining almost every solid material. The quality of laser machining depends on the processing parameters that dictate material ablation mechanisms. The understanding of the complex physics associated with ultrashort pulsed laser (USPL) material interaction and ablation has advanced significantly owing to a great many theoretical and experimental studies in the past 20 years. To date, USPLs have been considered as a novel tool for micro- and nano-machining of bulk or thin film materials and for internal modification of transparent materials via multi-photon absorption in a tiny focal volume. Moreover, USPL material processing is now gaining interest in other applications, such as in sensors, electronics and medical device industries.

Keywords: pulsed laser, femtosecond laser, laser material ablation, two-temperature model, LIPSS

1. Introduction

Since the first laser was invented in 1960, many different types of lasers have been developed due to rapidly increasing areas of applications. In the selection of a laser for a particular application, the following parameters are usually considered: pulse duration, wavelength, fluence, pulse repetition rate, beam uniformity and stability, bandwidth, weight and size of laser system, lifetime and reliability, hardware design, and cost. Among them, the first five are more crucial for material processing. Sufficient laser pulse energy and proper repetition rate (if a pulse laser is selected) are needed for processing the material, wavelength that determines laser energy absorption, and pulse duration that controls the heat affected zone. The interaction among the above four effects, together with the beam quality, controls the material process quality.

Ultrashort pulsed lasers (USPLs) are a particular class of lasers whose pulse duration (t_p) is less than a few picoseconds (ps). This classification is based on the fact that for most solids the time to establish thermal equilibrium between electrons and phonons is of the order of picoseconds. For a 100 femtoseconds (fs) and 0.1 J laser pulse, for example, the peak power is one terawatt (1.0×10^{12} W). If the laser pulse is focused onto an area of 0.1 mm^2, its peak intensity can reach 10^{15} W/cm^2. In view of the extremely short pulse duration and high intensity, USPLs have been explored and demonstrated great potential for a large variety of applications in physics, chemistry, life science, materials, and engineering science in the past 20 years.

Ultrashort time and high peak power are the two unique features of USPLs such that a thin layer of material can be ablated before the absorbed laser energy diffuses into the surrounding bulk. Because of that, a material can be processed very precisely with minimal or even without collateral damage. Such concepts and applications to micro/nano precision processing have been demonstrated in laboratories since the mid-1990s. Furthermore, with the possibility of reaching an extremely high intensity by focusing ultrashort pulses in a tiny volume or area, multi-photon absorption is another niche that makes USPLs well suited for 3D micro and nano processing and fabrication. The advantages of USPL material processing include: (i) high precision [1, 2], (ii) minimal collateral damage, (iii) capability of processing practically any material, (iv) 3D fabrication [3–5], and (v) a single step for creating different surface structures, such as laser-induced periodic surface structures (LIPSS) [6]. Larger material removal rates than those with conventional pulsed lasers by ultrafast bursts of pulses have also been reported recently [7].

In this chapter, three areas of laser material processing are considered: (a) mechanisms of laser-material interaction and ablation, (b) modeling of laser material ablation, and (c) applications. For the mechanisms, the characteristic times of materials and the difference in material interactions with long, short and ultrashort laser pulses are discussed. The modeling is limited to laser-material interaction for metal and semiconductor materials, including ablation for metals and damage for semiconductors. Examples of the USPL application focus on modification of material properties below the surface of transparent materials and LIPSS for sensors, precision molds, and medical devices.

2. Mechanisms of laser-material interaction and ablation

The mechanisms of laser-material interaction and ablation mainly depend on the characteristic times and thermophysical properties of materials as well as laser parameters such as wavelength, pulse duration and fluence. This section will focus on laser interactions with industrial materials.

2.1. Laser interaction with metals

Laser irradiation to a metal solid is a two-step heating process [8]. The incident photons collide with free electrons that are confined within the laser light propagation path. The absorbed laser energy is then converted to kinetic energy of the excited electrons, allowing them to travel

relatively long distance (tens or hundreds of nanometer (nm), depending on the materials) before collisions with other electrons. This is referred to as ballistic electron transport in metals. After the electron-electron collisions, their kinetic energy is spread among the electrons into the Fermi-Dirac distribution. This phase is referred to as thermalization, and is completed in a few tens of femtoseconds. The electron temperature (T_e) is measureable at this time. Afterwards, the electron thermal energy diffuses, through electrons, into a deeper part of the material. In the meantime, a part of the electron thermal energy is transferred to lattice (phonons) through electron-phonon collision. It takes few picoseconds (ps) for the excited phonons to become thermalized so that the lattice temperature (T_l) can be measured. The energy exchange between the electrons and the lattice lasts for tens or hundreds of picoseconds, leading to thermal equilibrium ($T_e = T_l$) between the two subsystems (electrons and lattice), then common thermal diffusion drives the heat dissipation in the bulk.

During pulsed laser irradiation, since the heat capacity of electrons is about two orders of magnitude lower than that of the metal lattice, the electron temperature can shoot up to a very high temperature (e.g., 10^3–10^4 K) while the lattice mainly remains in low temperature state. Hence, the electron and lattice temperatures can be quite different before thermal equilibrium is established. This two-step heating is particularly true for laser pulses that are shorter than 100 ps [8, 9]. **Figure 1** shows the time histories of the calculated electron and lattice temperatures at the irradiated surface of a copper foil by a single femtosecond laser pulse (duration 120 fs, wavelength 800 nm) of two fluences (0.5 J/cm^2 and 3.0 J/cm^2). The smooth evolutions of both T_e and T_l with the time shown in the case of a laser fluence of 0.5 J/cm^2 are the same as

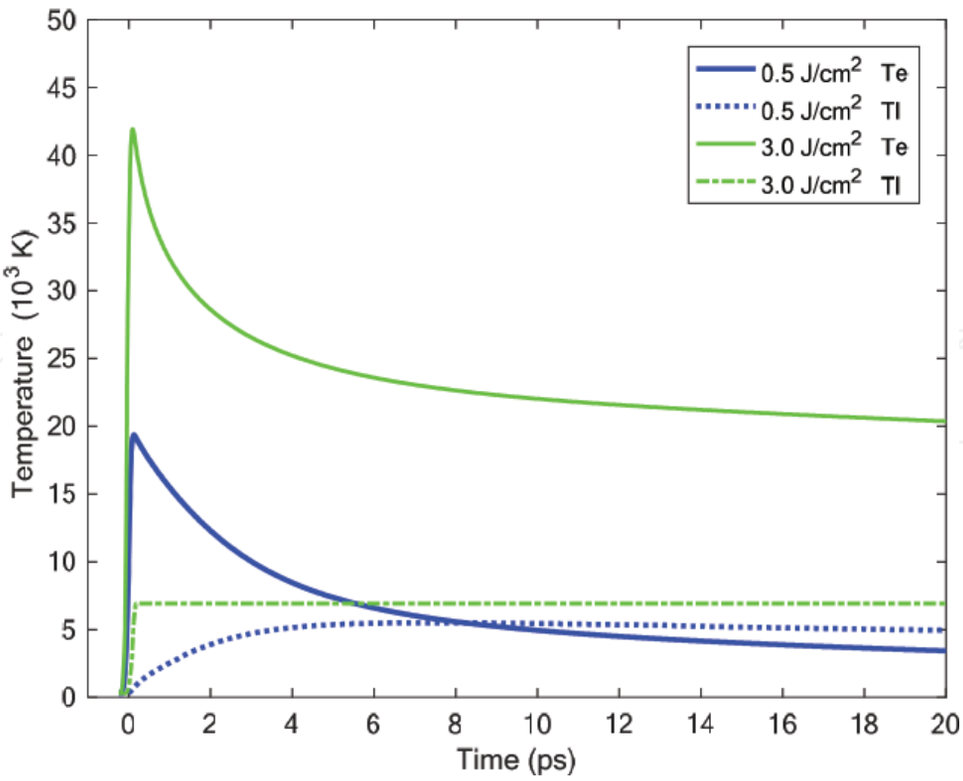

Figure 1. Calculated electron and lattice temperatures as functions of time.

most simulation results of USPL heating reported previously. For heating by nanosecond (ns) or longer laser pulses, since the characteristic times of energy transfer between the excited electrons and lattice are much shorter than the laser pulse duration, thermal equilibrium between the two subsystems is nearly established while lasing. This is particularly true for laser pulses longer than 10 ns [10]. Therefore, one-step heating ($T_e = T_l$) is usually considered for the case of conventional, long-pulse laser heating.

2.2. Laser ablation of metals

The laser energy is primarily deposited within the optical penetration depth (a few tens of nm for metals) with an exponential decay. Because the penetration depth is so shallow, the gradient of the induced electron temperature during and shortly after USPL irradiation can be immense. This non-uniform electron temperature can generate a considerably large hot-electron blast force that could cause severe deformation in the cold lattice [9–12]. The non-uniform lattice temperature that develops later is another cause for the ultrafast deformation. Due to the small size of the affected thermal zone, the gradient of lattice temperature could be very sharp. As a result, severe thermal stresses are induced in the lattice. In the case of a relatively low laser fluence, the hot-electron blast force and thermal stress are the vital power that destroys the bulk material underneath the irradiated surface before the thermal energy is significantly conducted into the bulk [11, 13]. For high laser fluences, the lattice, on the other hand, can be superheated and subsequently undergo a metastable phase transformation from solid to liquid and then, further to vapor if the fluence is sufficiently high [14–17].

Using a simple criteria for material removal, Momma et al. [2] and Nolte et al. [18] deduced two well-known logarithmic functions for the USPL material ablation depth: $\delta = \eta \ln(F_o / F_{th}^{\eta})$ for low fluences and $\delta = \zeta \ln(F_o / F_{th}^{\zeta})$ for high fluences, where η is the optical penetration depth; ζ is the effective electron heat diffusion length; F_o is the laser fluence; and F_{th}^{η} and F_{th}^{ζ} are the ablation threshold for low and high laser fluences, respectively. The failure of these two simple functions to describe the ablation rate for higher fluences [19] suggests that more mechanisms may be involved in the ablation process.

For USPL heating at laser fluences slightly exceeding the ablation threshold, only a thin layer of material is ablated by a single pulse due to the effects of the hot-electron blast and/or thermal expansion. Material ablation can take place during the lasing or after the laser pulse is off but before the next pulse arrives. When the material is removed, its associated thermal energy is also eradicated. Because very little or no molten liquid remains in the bulk material, hydrodynamic motion is negligible or never even occurs. As a result of a very thin layer ablated with little or no thermal damage to the bulk material by each laser pulse, the hole or crater resulting from this non-thermal ablation process can be very clean and precise [2].

Although non-thermal ablation can precisely process materials with minimal damage, it suffers from its very slow processing due to insufficient laser energy. This, therefore, creates a need for developing a more efficient means of processing. One potential approach to efficiently process a material target, for example, is to use a laser beam that irradiates high-fluence pulses

http://dx.doi.org/10.5772/intechopen.70454

(for high ablation rate) and then, is followed by relatively low-fluence pulses (for high precision). One can consider the low-fluence finishing as an "integrated" processing step, which results in high quality without the need for a separate post-processing. **Figure 2** shows the excellent quality of a hole produced by a femtosecond laser beam of 120 fs and 800 nm with low-fluence finishing.

For laser fluences well exceeding the ablation threshold, non-thermal ablation only occurs in the early time of the USPL heating [11]. Because the lattice temperature rises so drastically, the irradiated material rapidly undergoes phase transformation. Due to the fact that time is too short to allow necessary heterogeneous nuclei to form, the melted material is unable to boil [14, 20]. Instead, it is superheated past the normal boiling point to more or less the thermodynamic equilibrium critical temperature (T_{tc}). At that state, the tensile strength of the superheated liquid falls to zero and fluctuation in volume becomes dramatic, leading to a tremendous number of homogeneous nuclei being formed. As a result of the bubbles formed at such an extremely high rate, the subsurface layer of metastable liquid relaxes explosively into a mixture of vapor and equilibrium liquid droplets, which are immediately ejected from the bulk material. This thermal ablation mechanism is referred to as phase explosion. The phase explosion and material removal of metals caused by nanosecond [15] and USPL [16, 17, 21–23] heating have widely been investigated experimentally and theoretically. However, most studies investigated the thermal ablation within a low laser fluence regime (e.g., <10 J/cm^2), and a high laser fluence regime was rarely investigated.

As discussed above, high stress (non-thermal) and phase explosion (thermal) are the two main mechanisms for metal ablation. Non-thermal ablation provides a precision controllability which is crucial to micro- and nano-scale material processing. Another advantage is that little or no post processing is needed. Therefore, USPLs with a fluence slightly exceeding the ablation threshold are a good choice for microfabrication for which precision and small sizes are required. On the other hand, USPLs with fluences well beyond the ablation threshold may not offer an advantage for precise material processing due to the strong thermal (superheating and bubble forming) and mechanical (fluid ejection) effects that accompany them. However, there could be a trade-off between precision and efficiency of laser material processing [18].

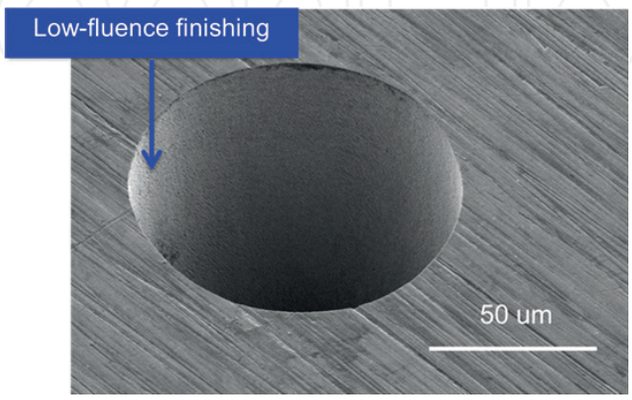

Figure 2. Drilling of aluminum by a femtosecond laser beam of 120 fs and 800 nm with low-fluence finishing.

The LIPSS created on a metal surface by multiple ultrashort laser pulses with a fluence near the ablation threshold are another interesting result of laser matter interaction [6]. Formation of micro- and nano-sized periodic ripples and column arrays are dependent on the number of laser pulses, pulse duration, fluence, wavelength, radiation polarization, and the ambient conditions. The formation of periodic-like surface structures on metal can be attributed to the interference between an incident femtosecond laser beam and the surface scattered wave [24–27].

2.3. Laser interaction with semiconductor and dielectric materials

The difference between semiconductor and dielectric materials is the number of free electrons in the conduction band. When a semiconductor or dielectric material is irradiated by a laser, the electrons in the valence band absorb the photon energy and then transit to the conduction band via single- or multi-photon absorption, depending on the photon energy (hv, where h is the Planck constant and v is the laser-light frequency) and the band-gap energy (E_g) of the material. The interband transition of the electrons creates holes in the valence band. The excess energy of the created electron-hole pairs, $khv - E_g$ ($k = 1$ for single-photon absorption and $k > 1$ for k-photon absorption), is the kinetic energy of the excited carriers that determines the carrier temperature. As the electrons and holes undergo temporal and spatial evolution, some of them recombine, for example, through the three-body Auger process. Meanwhile, additional electron-hole pairs could be generated via impact ionization from those free carriers with kinetic energy that is equal to or greater than the band gap. The excited electron-hole pairs thermalize to the Fermi-Dirac distribution via carrier-carrier collisions on a <100 fs timescale after photon absorption. In the meantime, thermalization between the carriers and phonons proceeds until the thermal equilibrium state is inevitably established.

2.4. Laser ablation of semiconductor and dielectric materials

Three main factors that affect damage and ablation of semiconductor and dielectric materials by lasers are: (a) free-electron density, (b) free-electron kinetic energy, and (c) carrier and phonon temperature. Increasing of the carrier and phonon temperature leads to the hot-electron blast force, thermal expansion, superheating, and phase explosion that are basically the same as those in metal materials described previously.

At the very beginning of USPL excitation, the density rise of the electron-hole pairs generated grows exponentially after a very short transient [28]. Depending on the peak laser intensity, for example, 12 TW/cm^2, this could result in a high density (10^{21}–10^{22} cm^{-3}) of the electron-hole pairs. When the kinetic energy of an excited electron exceeds the surface barrier and the momentum component normal to the surface of the material is positive, the excited electrons can escape from the irradiated material into the surrounding air or vacuum. Consequently, the irradiated surface gains highly positive charges, leading to a repulsive force. If the repulsion force between ions is greater than the lattice binding strength, the atomic bonds are broken and a subsurface layer of the material is disintegrated. Damage and removal of material by this repulsive force is referred to as Coulomb explosion [29]. This ablation mechanism is non-thermal because Coulomb explosion occurs prior to significant heating of the phonon

subsystem. Like the non-thermal ablation in metals, this is the mechanism that can lead to high precision in processing semiconductor or dielectric materials with USPLs.

It is quite natural to use focused USPLs for 3D micromachining of semiconductor and dielectric materials because of their extremely high peak intensity. With the advantages of superior localization and great optical penetration depth (longer laser wavelength), multi-photon absorption, in general, is a better mechanism for 3D micromachining, especially for processing inside bulk material. One-photon absorption may only be suitable for surface processing due to linear absorption and smaller penetration depth (shorter laser wavelength).

When a USPL beam is tightly focused inside a transparent material, multi-photon ionization, tunneling ionization, and avalanche ionization could occur in the focal volume. Like metals, the excited electrons transfer their energy to the ions via collision. With some time delay, the electrons and ions eventually reach thermal equilibrium. When the laser intensity is below a certain threshold, electrons recombine with holes in a non-radiative way. For laser intensities exceeding the certain level (referred to as plasma threshold), a plasma spark, resulting from the recombination of high-density electron plasma with holes, can be observed. The spark is associated with an optical breakdown of the transparent materials, having a characteristic duration of the order of 10 ns. After recombination, the thermal energy diffuses away from the focal volume on a microsecond timescale. At even higher intensities, laser-induced permanent modification of material properties is observed [4]. If the laser intensity is above the modification threshold, the hot electron-hole plasma and ions explosively expand from the focal volume into the surrounding material.

With tight focusing of ultrashort laser pulses, different kinds of permanent structure changes in a transparent material can be made by adjusting the incident pulse energy, in principle. Fabrication/machining/processing can be performed on the surface or within the bulk of the material by moving the laser focus along the desired paths. More detailed information can be found in the papers cited in the review paper [30].

3. Modeling of laser material ablation

In this section, we focus on two-step heating models for ultrafast thermal transport, ablation models for metals, and damage models for semiconductor materials.

3.1. Two-temperature model for metals

The two-temperature (2T) model was pioneered by Anisimov et al. [31] in 1974 to describe a two-step heating process of metals subjected to short-pulse laser irradiation. It was not until the early 1990s that USPL material interactions received considerable attention. Since then, numerous modified versions of 2T have been proposed [9, 32]. Based on the Boltzmann transport approximation, a semi-classical 2T model is derived for the dynamics of electron concentration (n), mean (drift) velocity ($\overline{v}_e$), and average energy for metal materials [9]:

$$\frac{\partial n}{\partial t}+\nabla\cdot\left(n\bar{v}_e\right)=0 \tag{1}$$

$$m_e\frac{\partial\bar{v}_e}{\partial t}+m_e\bar{v}_e\cdot\nabla\bar{v}_e+\left[k_B\left(1+\frac{T_e}{C_e}\frac{\partial C_e}{\partial T_e}\right)-e\beta_e\right]\nabla T_e=-\frac{eT_e\bar{v}_e}{\mu_o T_l} \tag{2}$$

$$C_e\left(\frac{\partial T_e}{\partial t}+\bar{v}_e\cdot\nabla T_e+\frac{2}{3}T_e\nabla\cdot\bar{v}_e\right)+\nabla\cdot\overline{Q}_e=-G\left(T_e-T_l\right)+S \tag{3}$$

In the above equations, m_e is the electron mass, $\overline{Q}_e$ is the heat flux vector in the electron subsystem, k_B is the Boltzmann constant, e is the electron charge, μ_o represents the mobility of the electrons, β_e is the temperature-dependent parameter for free electrons, C_e is the heat capacity of the electron, G represents the electron-phonon coupling factor, S is the volumetric laser heat source, and ∇ is the divergence operator. Since the electron relaxation time of metals is around ten femtoseconds, the constitutive relation for $\overline{Q}_e$ and T_e is given by [32]:

$$\tau_e\frac{\partial\overline{Q}_e}{\partial t}+\overline{Q}_e=-K_e\nabla T_e \tag{4}$$

where τ_e is the electron relaxation time (the mean time for electrons to change their states), and K_e is the electron thermal conductivity.

For the lattice subsystem, the thermal transport equation includes an energy exchange with the electrons and a thermal relaxation effect in a general case [33]:

$$C_l\frac{\partial T_l}{\partial t}=-\nabla\cdot\overline{Q}_l+G\left(T_e-T_l\right) \tag{5}$$

$$\tau_l\frac{\partial\overline{Q}_l}{\partial t}+\overline{Q}_l=-K_l\nabla T_l \tag{6}$$

In Eqs. (5) and (6), $\overline{Q}_l$ is the heat flux vector in the lattice, τ_l is the relaxation time in phonon collisions, and C_l and K_l are the heat capacity and thermal conductivity of lattice, respectively.

By neglecting the electron drift velocity, energy equation (3) is simplified to:

$$C_e\frac{\partial T_e}{\partial t}=-\nabla\cdot\overline{Q}_e-G\left(T_e-T_l\right)+S \tag{7}$$

Thus, the semi-classical 2T model, seen in Eqs. (1)–(6), is reduced to the dual-hyperbolic 2T model (HH2T) [33].

For pure metals, K_l is much smaller than K_e. The hyperbolic 2T model (H2T) [32] can be retrieved from the HH2T model by neglecting the heat conduction in the lattice, i.e., $\nabla\cdot\overline{Q}_l=0$ in Eq. (5). Further neglecting the electron relaxation effect in the H2T model leads to the parabolic 2T model (P2T) [8, 34].

After the thermal equilibrium, $T_e = T_l = T$, $\overline{Q}_e + \overline{Q}_l = \overline{Q}$, $C_e + C_l = C$, and $K_e + K_l = K$. Combining Eqs. (5) and (7) yields the macroscopic energy balance equation:

$$C\frac{\partial T}{\partial t} = -\nabla \cdot \overline{Q} + S \tag{8}$$

The above energy equation (8) together with Fourier's heat conduction law is a well-known, parabolic one-temperature heat conduction model (P1T). When the Cattaneo equation [35] is considered, the result becomes a hyperbolic (thermal wave) one-temperature model (H1T). The above 1T models represent one-step heating and have been widely used for long-pulse laser heating since the electrons and lattice are assumed to be in thermal equilibrium instantaneously when a medium is heated.

The thermophysical properties, *C*, *K* and *G*, control thermal response in laser-irradiated material. The expressions for these three thermophysical properties can be found in Refs. [10, 36]. Recently, Lin et al. [37] presented data C_e and *G* for different metals over a wide range of electron temperatures from room temperature to 5×10^4 K. A formula for K_e up to Fermi temperature was given by Anisimov and Rethfeld [38].

The mechanical stresses caused by the hot-electron blast force and the thermal stresses induced by non-uniform temperatures in the lattice can be solved by the equation of motion of lattice:

$$\rho_l \frac{\partial^2 u_i}{\partial t^2} = \sigma_{ij,j} + \frac{2}{3}(C_e T_e)_{,i} \tag{9}$$

where u_i ($i = x$, y, and z) is the displacement vector of a material (lattice) point, σ_{ij} is the stress tensor at the point, and the subscript "," denotes the spatial derivative. The last term on the right-hand side of Eq. (9) is the hot-electron blast force. The thermal strains resulting from a non-uniform lattice temperature are included in the stress-strain relations. The deformation can be linearly elastic or non-linearly plastic.

The exchange of thermal and mechanical energy should not be neglected due to the extremely high strain rate (~10^9 s^{-1}). Thus, the energy equation of lattice, Eq. (5), is re-written as:

$$C_l \frac{\partial T_l}{\partial t} = -\nabla \cdot \overline{Q}_l + G(T_e - T_l) - (3\lambda + 2\mu)\varphi T_l \frac{\partial \varepsilon_{kk}}{\partial t} \tag{10}$$

where λ is the Lamé constant, μ is the shear modulus, φ is the thermal expansion coefficient, and ε_{kk} $(= \nabla \cdot \overline{u})$ is the volume dilatation. In addition, the strain rate effects on plastic deformation and failure could be substantial, and the existing stress-strain relations and fracture strength may be insufficient for ultrafast deformation. To accurately predict non-thermal material ablation by stresses, the strain rate effects on material behavior should be investigated further and quantified.

3.2. Laser heat source

The most popular laser beams are Gaussian in both space and time. For simplicity, let us consider an incident laser beam that is normal to the material target. The volumetric laser heat source *S* in Eqs. (3) and (7) is given as [39]:

$$S(r,z;t)=\sqrt{\frac{\beta}{\pi}}\frac{[1-R(r,0;t)]F_o}{t_p}\alpha(r,z;t)\exp\left[-2(\frac{r}{r_o})^2-\int_0^z\alpha dz-\beta(\frac{t-mt_p}{t_p})^2\right] \quad (11)$$

where r is the radial distance from the center of the beam, z is the coordinate in the direction of laser beam propagation, $F_o = J_o/(\pi r_o^2/2)$ with J_o denoting the pulse energy, r_o being the beam radius defined at the e^{-2} distance, $R(r, 0; t)$ is the surface reflectivity of the material, α is the absorptivity coefficient, t_p is the full width half maximum (FWHM) of the Gaussian temporal pulse, m is an integer, and $\beta = 4\ln(2)$. The lasing, assumed to start at $t = 0$, reaches its peak power at $t = mt_p$, and ends at $t = 2mt_p$. The value of m can be set at 2 or 3 since the laser energy outside this period of time is inconsequential. If the effects of the hot electrons ballistic motion [40] are taken into account, the laser heat source is modified to:

$$S(r,z;t)=\sqrt{\frac{\beta}{\pi}}\frac{[1-R(r,0;t)]F_o}{t_p}\frac{1}{\delta(r,z;t)+\delta_b(r,z;t)}\exp\left[-2(\frac{r}{r_o})-\int_0^z\frac{1}{\delta+\delta_b}dz-\beta(\frac{t-mt_p}{t_p})^2\right] \quad (12)$$

where $\delta = 1/\alpha$ is the temperature-dependent optical penetration depth and δ_b is the ballistic electron penetration depth. The temperature-dependent optical properties, R and α, in Eqs. (11) and (12) can be determined from optical properties and the Fresnel function.

Recently, an extended Drude model [41] was proposed to characterize the temperature-dependent R and α, and a critical point model with three Lorentzian terms for interband transition [42] for copper. The numerical results show that when a metal is irradiated by a USPL at high fluence, the dynamic changes of R and α during the laser irradiation could significantly alter laser energy absorption and the distribution of laser heat density. Although it is only true for low electron temperatures, the constant R and α at room temperature have been widely employed in 2T modeling. In this case, the integral term becomes a constant, z/δ in Eq. (11) and $z/(\delta + \delta_b)$ in Eq. (12).

3.3. Comparison of different thermal models

Figure 3 compares the predictions of four thermal models, HH2T, H2T, H1T, and P1T, for lattice temperatures at the front surface of a 200 nm gold film heated by a laser pulse of F_o = 0.5 J/cm^2 and t_p = 100 ps and 1 ns [10]. Evidently, both of the one-temperature models significantly overestimated the bulk temperature for the 100 ps pulse; hence, they are inadequate for simulating USPLs heating. The results, shown in **Figure 3(b)**, confirm that the Fourier heat conduction model is sufficient for long-pulse laser heating. In fact, the difference among the four models becomes indistinct for a 10 ns laser pulse [10].

3.4. Ablation models for metals

The 2T models discussed above only characterize thermal transport in a solid metal. For material ablation, other physical processes such as phase transitions and material removal need to be considered. Different approaches have been proposed to simulate laser material ablation, including ultrafast thermoelasticity [11], dynamics of thermal ablation [17], hydrodynamic modeling [43], molecular dynamics [22], etc. Although those numerical analyses [17]

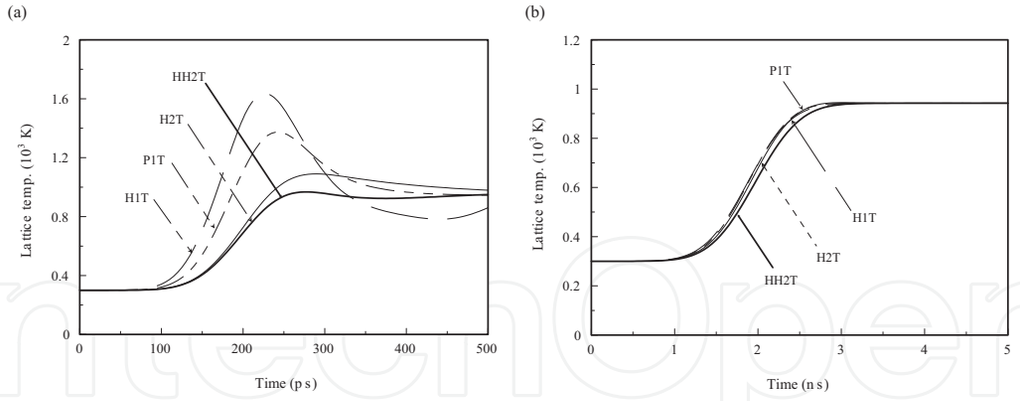

Figure 3. Comparison of the four thermal model predictions for lattice temperature at the front surface of a 200 nm gold film heated by a laser pulse of F_o = 0.5 J/cm^2 and (a) t_p = 100 ps and (b) t_p = 1 ns. Reproduced with permission from publisher [10].

show a certain degree of success in comparison with experimental measurements, none of the aforementioned models have been validated thoroughly with experimental data for USPL ablation over a wide pulse duration and fluence.

A comprehensive USPL ablation model is needed to be able to accurately describe the entire ablation process and predict the ablation depth and rate. It should be developed based on universal regulations and methods that allow for the description of non-equilibrium responses and cover the complex physical phenomena for the entire laser process. Such phenomena include photon-electron interaction, laser-pulse propagation and ionization, phase transitions, superheating through a metastable liquid phase, rapid nuclei formation, explosion and dynamics of homogeneous nuclei (bubbles), generation of recoil pressure, hydrodynamic motion, formation and dynamics of the plasma plume, laser-plasma interaction, radiation from the resulting plasmas, condensation and re-solidification of the liquid/vapor, etc.

To accurately simulate thermal ablation by USPLs, a semi-classical 2T model integrated with models of phase transformations for ultrafast melting, evaporation and re-solidification and a phase explosion model for ejection of metastable liquid and vapor was attempted recently [44]. When superheated liquid temperature reaches $0.9T_{tc}$, phase explosion is assumed to take place [20] and that material, including both electrons and lattice, is then removed under the assumption of phase explosion. Once phase explosion no longer occurs, vaporization could continue until the lattice temperature drops significantly. **Figure 4** shows the time history of the ablation depth for copper foil irradiated by a single femtosecond laser pulse (duration 120 fs, wavelength 800 nm) of different fluences. The steep occurrences of material ablation result mainly from phase explosion, while the sloping parts result from vaporization. As shown in **Figure 4 (b)** for the case of laser fluence 6.1 J/cm^2, the ablation depth by phase explosion and vaporization are 258.4 nm (up to 310 ps) and 5.9 nm (from 310 to 600 ps), respectively. The results shown here indicate that for high fluences, phase explosion is the dominating material ablation mechanism in USPL material ablation. It is noted that this ablation model is not yet fully comprehensive.

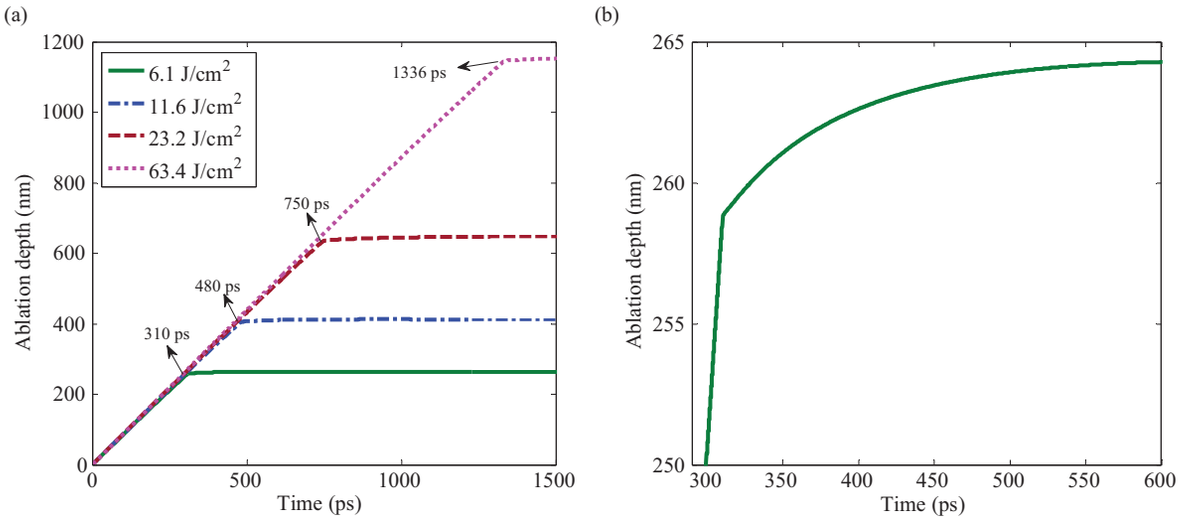

Figure 4. (a) Time histories of the ablation depths of a copper foil by a single femtosecond laser pulse (duration 120 fs, wavelength 800 nm) of different fluences, (b) magnification of the fluence case of 6.1 J/cm^2. Reproduced with permission from publisher [45].

3.5. Ultrafast transport dynamics models for semiconductors

To model the transport process of a large number of hot electrons, holes, and phonons in a semiconductor, the formalism must be based on the principle of statistical mechanics. A self-consistent model for transport dynamics in semiconductors caused by USPL heating can be found in [46]. Based on the relaxation-time approximation of the Boltzmann equation, the rate equations are derived for the dynamics of electron-hole carrier number density and current, ambipolar energy current, carrier energy, and lattice energy.

3.5.1. Rate equation for carrier pairs

The balance equation for the electron-hole pairs number density generated by a laser pulse for two-photon absorption is:

$$\frac{\partial n}{\partial t} = \frac{\beta_1 I(x,t)}{h\nu} + \frac{\beta_2 I^2(x,t)}{2h\nu} - \gamma n^3 + \theta n - \nabla \cdot J \tag{13}$$

where β_1 is the avalanche coefficient, β_2 is the 2-photon absorption coefficient, γ is the Auger recombination coefficient, θ is the impact ionization coefficient, and J is the carrier current. The magnitude of β_1 is much greater than that of β_k ($k > 1$). For silicon at room temperature, for instance, $\beta_1 = 1.0 \times 10^4\ cm^{-1}$ and $\beta_2 = 2.0 \times 10^{-9}\ cm/W$. The last three terms on the right-hand side of Eq. (13) represent Auger recombination, impact ionization, and the loss due to carrier current, respectively. The Auger recombination is described as the time when an electron-hole pair recombines, giving up its energy to a third electron in the conduction band; this reduces the carrier number density. The reverse effect is impact ionization. Due to the nonlinearity nature (I^k), multi-photon absorption could be more efficient and occur faster than single-photon absorption when laser intensities are sufficiently high.

3.5.2. Rate equation for carrier energy

The balance equation for the electron-hole pairs energy produced by a laser pulse for two-photon absorption is:

$$C_{e-h}\frac{\partial T_e}{\partial t}=\left(\beta_1+\Theta n\right)I(x,t)+\beta_2 I^2(x,t)-\nabla\cdot W-\frac{C_{e-h}}{\tau_e}(T_e-T_l)$$
$$-\frac{\partial n}{\partial t}\left\{E_g+\frac{3}{2}k_B T_e\right\}-n\left(\frac{\partial E_g}{\partial n}\frac{\partial n}{\partial t}+\frac{\partial E_g}{\partial T_l}\frac{\partial T_l}{\partial t}\right) \tag{14}$$

where C_{e-h} is the heat capacity of electron-hole pairs, Θ is the free carrier absorption cross-section, and W is the ambipolar energy current which is the sum of the carrier energy currents in electrons and holes.

3.5.3. Rate equation for lattice energy

For semiconductor materials the thermal conductivity of the lattice is comparable with the bulk value. It is necessary to consider the thermal transfer in the lattice. The lattice energy rate is expressed as:

$$C_l\frac{\partial T_l}{\partial t}=\nabla\cdot\left(k_l\nabla T_l\right)+\frac{C_{e-h}}{\tau_e}(T_e-T_l) \tag{15}$$

The three rate equations (13)–(15), together with the constitutive equations for the carrier pair current and the ambipolar energy current [46], compose a complete self-consistent model for ultrafast transport dynamics in semiconductors subjected to USPL irradiation.

Figure 5 shows the time histories of the density and temperature of carriers and the lattice temperature at the incident surface of a silicon sample irradiated by a 500 fs laser pulse with fluence 0.005 J/cm^2 [46]. The peak laser power is at t = 1.5 ps (m = 3). As shown in **Figure 5**, the carrier temperature reaches its maximum at about 0.68 ps and the number density reaches its maximum at about 2.21 ps. It should be noted that when the peak carrier temperature occurs, the laser power is only at about 0.06% of its maximum. The contradictory intuition of this high temperature is attributed to a very small amount of electron-hole pairs that are created during this early time. Consequently, the carrier heat capacity is very small, thereby leading to a rapid, noticeable rise in the carrier temperature although the net carrier thermal energy is quite low. As time is prolonged, the carrier density increases drastically since much more laser energy has been absorbed. As a result, the carrier heat capacity becomes greater and greater. Meanwhile, the energy loss, due to the change in carrier energy density (the second last term on the right hand side of Eq. (14)), becomes pronounced, and so does the loss due to thermal transfer from the carriers to the lattice. Those changes make the rate of change of the net energy unable to remain positive at some point and thereafter, even though considerable laser energy is absorbed. This explains why the carrier temperature quickly reaches its peak very early in the laser irradiation and then falls. The numerical result in Ref. [46] also shows that one-photon absorption and Auger recombination are two crucial factors that alter the carrier's number density.

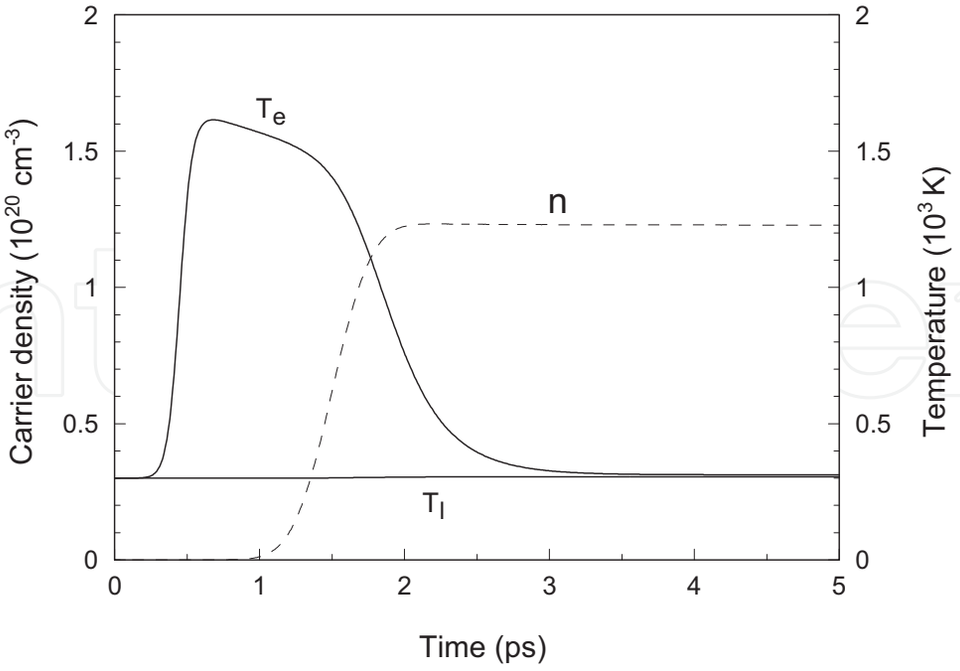

Figure 5. Time evolution of carrier density (n), carrier temperature (T_e), and lattice temperature (T_l) at the front surface of a 20 μm silicon sample heated by a 500 fs, 775 nm, 0.005 J/cm^2 laser pulse. Reproduced with permission from publisher [46].

3.6. Damage models for semiconductors

For pulse durations longer than the carrier–lattice energy relaxation time (a few picoseconds), it has generally been accepted that the solid–liquid phase transition by high laser fluences is a thermal (melting) process. On the other hand, experiments with femtosecond laser pulses of high fluence have demonstrated an ultrafast phase transformation on a subpicosecond time scale. The mechanism of this ultrafast phase transformation is nonthermal melting, differing from the above thermal melting.

Among the continuum models, there are two approaches that are frequently used in evaluation of the damage threshold for semiconductor materials. One approach employs a single rate equation to evaluate electron density in the conduction band [47]. The equation includes ionization rates for single and multi-photon absorption, avalanche ionization, and other relaxation terms. Damage is assumed when the calculated electron density exceeds a critical value, which is often determined semi-empirically by matching with the experimental data. In most cases, the critical value used differs from that of the critical density of electron-hole plasma that makes the plasma opaque (optical breakdown). The other approach uses a self-consistent model in which the rate equation for the carrier number density is coupled to the energy balance equations for both the carriers and phonons [46]. The onset of damage is determined by which condition, carrier number density, or lattice temperature is first met. **Figure 6** shows the comparison between the theoretical damage fluence thresholds with measured values for Si [9, 21]. It appears that the self-consistent model agrees fairly well with the experimental data for laser pulse durations up to several picoseconds; on the other hand, the carrier density model is only in good agreement for laser pulse durations of subpicoseconds [46]. In view of

http://dx.doi.org/10.5772/intechopen.70454

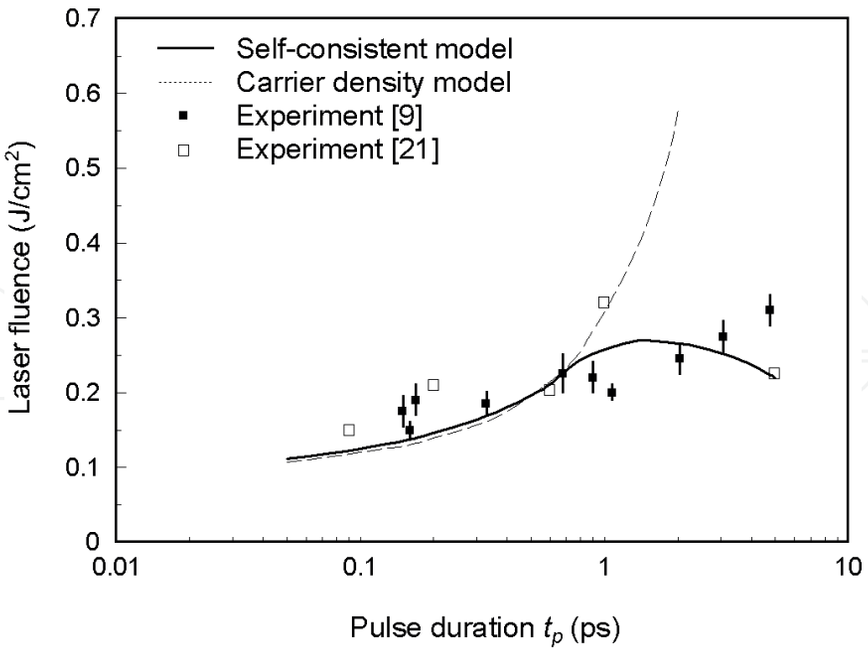

Figure 6. Theoretical and experimental damage thresholds versus laser pulse duration for Si. Reproduced with permission from publisher [46].

both approaches failing to predict the damage fluence thresholds for longer laser pulses, a more robust model or approach is suggested.

Modeling of the non-thermal ablation of semiconductor materials via Coulomb explosion can be found in the study by Stoian et al. [29]. On the other hand, a comprehensive modeling of thermal ablation via phase explosion, to the authors' knowledge, has not yet been reported in open literature.

4. Applications

As aforementioned, the great applications of USPLs are attributed to two unique features: ultrashort pulse duration and extremely high intensity. The benefits of USPL material processing include high precision with a minimal heat affected zone, the ability to locally modify below the surface of transparent materials, the single step for creating different surface structures, etc. A great number of applications of USPLs have been proposed, for example, to industrial technologies and bio/medicine [48, 49]. Recently, applications of LIPSS have been of particular interest.

The ability to locally modify material properties below the surface of transparent materials is an important area of USPL application. One interesting example is the repair of a packaged.

TFT-LCD panel. In this repair, a femtosecond laser beam passes through the polarizer, glass substrate, and then, focuses on the color filter (color photoresist) corresponding to the hot pixels such that the phenomenon of nonlinear multi-photon absorption can be induced within

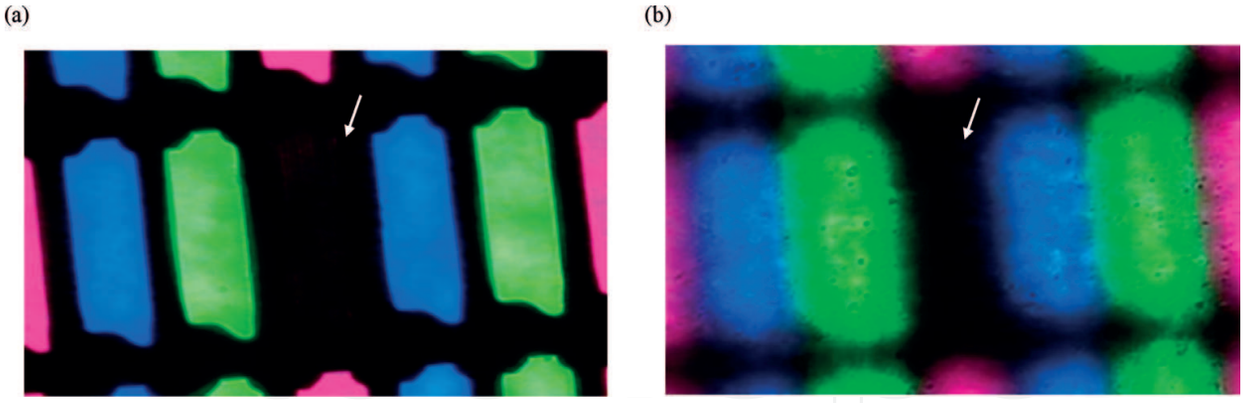

Figure 7. A red color filter after laser repair: (a) image focused at the photoresist and (b) image focused at the polarizer.

the localized area. Then, the property of the color photoresist layer is changed. The hot pixels become dead pixels, and any defective pixels inside the panel of the packaged LCD can be repaired directly. **Figure 7** shows a red colored filter after laser repair. The image is captured from different focal positions. As shown in **Figure 7(a)**, the red colored filter (marked by an arrow) has been blackened. In **Figure 7(b)**, however, the polarizer corresponding to the red colored filter (marked by an arrow) is not damaged after laser irradiation. Accordingly, the defective pixel is eliminated by the transformation of the bright one into a dark one.

LIPSS by USPLs allows for a new range of functionalized surface processing that permits novel applications for sensors, medical devices, precision molds, etc. For sensor applications, fabrication of Ag nanostructure-covered surface structures can be used for surface-enhanced Raman scattering (SERS) application. The SERS intensities of rhodamine 6G (R6G) at LIPSS-treated Ag substrates are 15 times greater than those at non-treated Ag substrates [50].

For medical devices applications, LIPSS by USPLs can be employed to fabricate electrosurgical blades [51, 52]. The average temperatures of tissue cut by conventional and LIPSS-treated electrosurgical blades are 145°C and 116°C, respectively. This corresponds to an improvement of about 29°C in temperature. As a result, there is less damage to tissue that is cut by the proposed electrosurgical blade.

LIPSS by USPLs is also employed to fabricate medical stainless steel [53]. As shown in **Figure 8**, the attachment assay with 72 h in a NIH3T3 culture demonstrates that significantly more cells are attached to the LIPSS-treated sample. This means that the cells spread over the treated surface more rapidly than over the non-treated surface. LIPSS-treated stainless steel is believed to possess better biocompatibility than stainless steel without surface modification.

For precision mold applications, for example, LIPSS by USPLs can be employed to fabricate structured molds and fast replication of large-area hierarchical micro/nano structures (lotus-leaf-like patterns) on a plastic part by injection molding [54]. Compared with an ordinary plastic surface, the contact angle of the structured plastic parts is increased by 38%, from 97 to 134°.

http://dx.doi.org/10.5772/intechopen.70454

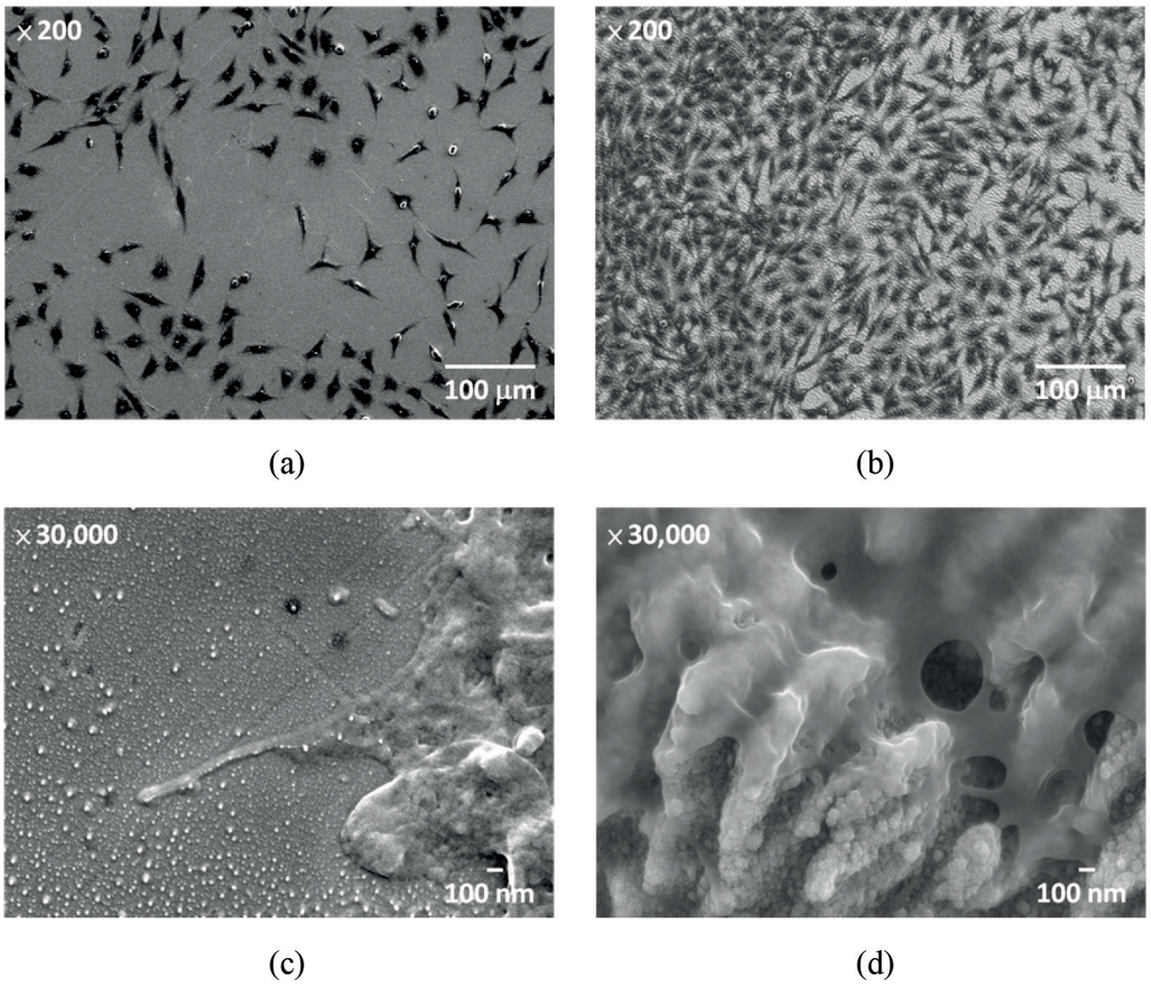

Figure 8. SEM images of an NIH3T3 cell after being in culture for 72 h: (a) control sample, (b) LIPSS-treated sample, (c) magnification of (a), and (d) magnification of (b). Reproduced with permission from publisher [53].

5. Conclusion

In reviewing laser micro- and nano-structuring of materials through pulse laser ablation, three main areas have been covered, including laser system development, experimentation and modeling, and applications. In this single chapter, we focused on laser material ablation mechanisms, modeling, and some applications of material properties modification and LIPSS that have been developed or demonstrated. Four areas in the modeling of laser matter interaction have been presented, including temperature response with temperature-dependent material properties and optical properties, ablation models for metals, ultrafast transport dynamics models for semiconductors, and damage models for semiconductors. Understanding the mechanisms and modeling of laser material interaction with materials can provide an insight for optimizing the processing parameters for precisely machining a variety of materials and can allow the development of high-value and innovative laser process techniques for a variety of applications.

Author details

Chung-Wei Cheng[1]* and Jinn-Kuen Chen[2]

*Address all correspondence to: weicheng@nctu.edu.tw

1 Department of Mechanical Engineering, National Chiao Tung University, Hsinchu, Taiwan

2 Department of Mechanical and Aerospace Engineering, University of Missouri, Columbia, USA

References

[1] Pronko P, Dutta S, Squier J, Rudd J, Du D, Mourou G. Machining of sub-micron holes using a femtosecond laser at 800 nm. Optics Communications. 1995;**114**:106-110

[2] Momma C, Chichkov BN, Nolte S, von Alvensleben F, Tünnermann A, Welling H, et al. Short-pulse laser ablation of solid targets. Optics Communications. 1996;**129**:134-142

[3] Davis KM, Miura K, Sugimoto N, Hirao K. Writing waveguides in glass with a femtosecond laser. Optics Letters. 1996;**21**:1729-1731

[4] Glezer E, Milosavljevic M, Huang L, Finlay R, Her T-H, Callan JP, et al. Three-dimensional optical storage inside transparent materials. Optics Letters. 1996;**21**:2023-2025

[5] Kawata S, Sun H-B, Tanaka T, Takada K. Finer features for functional microdevices. Nature. 2001;**412**:697-698

[6] Vorobyev AY, Guo C. Direct femtosecond laser surface nano/microstructuring and its applications. Laser & Photonics Reviews. 2013;**7**:385-407

[7] Kerse C, Kalaycıoğlu H, Elahi P, Çetin B, Kesim DK, Akçaalan Ö, et al. Ablation-cooled material removal with ultrafast bursts of pulses. Nature. 2016;**537**:84-88

[8] Anisimov SI, Kapeliovich BL, Perel'man TL. Electron emission from metal surfaces exposed to ultrashort laser pulses. Journal of Experimental and Theoretical Physics. 1974;**39**:375-377

[9] Chen J, Tzou D, Beraun J. A semiclassical two-temperature model for ultrafast laser heating. International Journal of Heat and Mass Transfer. 2006;**49**:307-316

[10] Chen J, Beraun J, Tham C. Investigation of thermal response caused by pulse laser heating. Numerical Heat Transfer: Part A: Applications. 2003;**44**:705-722

[11] Chen J, Beraun J, Grimes L, Tzou D. Modeling of femtosecond laser-induced non-equilibrium deformation in metal films. International Journal of Solids and Structures. 2002;**39**:3199-3216

[12] Chen J, Beraun J, Tham C. Ultrafast thermoelasticity for short-pulse laser heating. International Journal of Engineering Science. 2004;**42**:793-807

[13] Falkovsky L, Mishchenko E. Electron-lattice kinetics of metals heated by ultrashort laser pulses. Journal of Experimental and Theoretical Physics. 1999;**88**:84-88

[14] Miotello A, Kelly R. Laser-induced phase explosion: New physical problems when a condensed phase approaches the thermodynamic critical temperature. Applied Physics A: Materials Science & Processing. 1999;**69**:S67-S73

[15] Bulgakova N, Bulgakov A. Pulsed laser ablation of solids: Transition from normal vaporization to phase explosion. Applied Physics A: Materials Science & Processing. 2001;**73**: 199-208

[16] Dömer H, Bostanjoglo O. Phase explosion in laser-pulsed metal films. Applied Surface Science. 2003;**208**:442-446

[17] Chen J, Beraun J. Modelling of ultrashort laser ablation of gold films in vacuum. Journal of Optics A: Pure and Applied Optics. 2003;**5**:168

[18] Nolte S, Momma C, Jacobs H, Tunnermann A, Chichkov BN, Wellegehausen B, et al. Ablation of metals by ultrashort laser pulses. Journal of the Optical Society of America B-Optical Physics. Oct 1997;**14**:2716-2722

[19] Furusawa K, Takahashi K, Kumagai H, Midorikawa K, Obara M. Ablation characteristics of Au, Ag, and Cu metals using a femtosecond Ti: Sapphire laser. Applied Physics A. 1999;**69**:S359-S366

[20] Kelly R, Miotello A. Comments on explosive mechanisms of laser sputtering. Applied Surface Science. 1996;**96–98**:205-215

[21] Bulgakova NM, Bourakov IM. Phase explosion under ultrashort pulsed laser ablation: Modeling with analysis of metastable state of melt. Applied Surface Science. 2002;**197**:41-44

[22] Schäfer C, Urbassek HM, Zhigilei LV. Metal ablation by picosecond laser pulses: A hybrid simulation. Physical Review B. 2002;**66**:115404

[23] Leveugle E, Zhigilei L. Microscopic mechanisms of short pulse laser spallation of molecular solids. Applied Physics A. 2004;**79**:753-756

[24] Huang M, Zhao F, Cheng Y, Xu N, Xu Z. Origin of laser-induced near-subwavelength ripples: Interference between surface plasmons and incident laser. ACS Nano. Dec 2009;**3**:4062-4070

[25] Bonse J, Rosenfeld A, Krueger J. On the role of surface plasmon polaritons in the formation of laser-induced periodic surface structures upon irradiation of silicon by femtosecond-laser pulses. Journal of Applied Physics. Nov 15 2009;**106**:104910

[26] Hashida M, Namba S, Okamuro K, Tokita S, Sakabe S. Ion emission from a metal surface through a multiphoton process and optical field ionization. Physical Review B. 2010;**81**: 115442

[27] Huang M, Zhao F, Cheng Y, Xu N, Xu Z. The morphological and optical characteristics of femtosecond laser-induced large-area micro/nanostructures on GaAs, Si, and brass. Optics Express. Nov 8 2010;**18**:A600-A619

[28] Stuart BC, Feit MD, Herman S, Rubenchik AM, Shore BW, Perry MD. Optical ablation by high-power short-pulse lasers. JOSA B. 1996;**13**:459-468

[29] Stoian R, Ashkenasi D, Rosenfeld A, Campbell E. Coulomb explosion in ultrashort pulsed laser ablation of Al_2O_3. Physical Review B. 2000;**62**:13167

[30] Gattass RR, Mazur E. Femtosecond laser micromachining in transparent materials. Nature Photonics. 2008;**2**:219-225

[31] Anisimov S, Kapeliovich B, Perelman T. Electron emission from metal surfaces exposed to ultrashort laser pulses. Zhurnal Eksperimental'noi i Teoreticheskoi Fiziki. 1974;**66**:375-377

[32] Tien C, Qiu T. Heat transfer mechanism during short pulse laser heating of metals. American Society of Mechanical Engineers Journal of Heat Transfer. 1993;**115**:835-841

[33] Chen JK, Beraun JE. Numerical study of ultrashort laser pulse interactions with metal films. Numerical Heat Transfer Part A-Applications. Jul 2001;**40**:1-20

[34] Fujimoto J, Liu J, Ippen E, Bloembergen N. Femtosecond laser interaction with metallic tungsten and nonequilibrium electron and lattice temperatures. Physical Review Letters. 1984;**53**:1837

[35] Cattaneo C. A form of heat conduction equation which eliminates the paradox of instantaneous propagation. Compte Rendus. 1958;**247**:431-433

[36] Chen J, Latham W, Beraun J. The role of electron–phonon coupling in ultrafast laser heating. Journal of Laser Applications. 2005;**17**:63-68

[37] Lin Z, Zhigilei LV, Celli V. Electron-phonon coupling and electron heat capacity of metals under conditions of strong electron-phonon nonequilibrium. Physical Review B. 2008;**77**: 075133

[38] Anisimov SI, Rethfeld B. Theory of ultrashort laser pulse interaction with a metal. Proc. SPIE 3093, 1997; 192-203

[39] Wang S, Ren Y, Chang K, Cheng C, Chen J, Tzou D. Ablation of copper by a single ultrashort laser pulse. Journal of Laser Micro Nanoengineering. 2014;**9**:88-92

[40] Byskov-Nielsen J, Savolainen J-M, Christensen MS, Balling P. Ultra-short pulse laser ablation of copper, silver and tungsten: Experimental data and two-temperature model simulations. Applied Physics A-Materials Science & Processing. May 2011;**103**:447-453

[41] Ren YP, Chen JK, Zhang YW, Huang J. Ultrashort laser pulse energy deposition in metal films with phase changes. Applied Physics Letters. May 2011;**98**:191105

[42] Ren Y, Chen JK, Zhang Y. Optical properties and thermal response of copper films induced by ultrashort-pulsed lasers. Journal of Applied Physics. Dec 1 2011;**110**:113102

[43] Colombier JP, Combis P, Bonneau F, Le Harzic R, Audouard E. Hydrodynamic simulations of metal ablation by femtosecond laser irradiation. Physical Review B. Apr 2005;**71**: 165406

[44] Ren Y, Chen JK, Zhang Y. Modeling of ultrafast phase changes in metal films irradiated by an ultrashort laser pulse using a semiclassical two-temperature model. International Journal of Heat and Mass Transfer. 2012;**55**:1260-1627

[45] Cheng CW, Wang SY, Chang KP, Chen JK. Femtosecond laser ablation of copper at high laser fluence: Modeling and experimental comparison. Applied Surface Science. 2016;**361**: 41-48

[46] Chen J, Tzou D, Beraun J. Numerical investigation of ultrashort laser damage in semiconductors. International Journal of Heat and Mass Transfer. 2005;**48**:501-509

[47] Sokolowski-Tinten K, von der Linde D. Generation of dense electron-hole plasmas in silicon. Physical Review B. 2000;**61**:2643

[48] Fermann ME, Galvanauskas A, Sucha G. Ultrafast Lasers: Technology and Applications. Vol. 80. CRC Press; 2002

[49] Dausinger F, Lichtner F, Lubatschowski H. Femtosecond Technology for Technical and Medical Applications. Vol. 96. Springer Science & Business Media; 2004

[50] Chang H-W, Tsai Y-C, Cheng C-W, Lin C-Y, Lin Y-W, Wu T-M. Nanostructured Ag surface fabricated by femtosecond laser for surface-enhanced Raman scattering. Journal of Colloid and Interface Science. Aug 1 2011;**360**:305-308

[51] Cheng CW, Lin CY, Tseng WP, Ou KL, Peng PW. Electrosurgical unit with micro/nano structure and the manufacturing method thereof. ed: Google Patents; 2013

[52] Cheng CW, Lin CY, Wu PH, Chang KP, Horng JB, Wu WT, et al. Novel applications by femtosecond laser in electronics and medical device industries. In: Presented at the Smart Laser Processing Conference Yokohama, Japan; 2014

[53] Lin CY, Cheng CW, Ou KL. Micro/nano-structuring of medical stainless steel using femtosecond laser pulses. Physics Procedia. 2012;**39**:661-668

[54] Wu PH, Cheng CW, Chang CP, Wu TM, Wang JK. Fabrication of large-area hydrophobic surfaces with femtosecond-laser-structured molds. Journal of Micromechanics and Microengineering. 2011;**21**:115032

IntechOpen